A Multi-Target Electric Field Location Algorithm for Underwater Electrosense Robots Based on Sparse Bayesian Learning

Shuo Li[1], Renhui Fan[1], Guangyu Jiang[1], Yi Rong[1], Binya Han[1], Zicai Zhu[1] and Qiao Hu[1,*]

[1]Xi'an Jiaotong University, 28 Xianning West Road, Xi'an 710049, China

Abstract: Extremely Low Frequency (ELF) electric field signal provides a novel and promising solution to the target location problem due to its strong resistance to jamming and long propagation range. However, conventional algorithms such as Multiple Signal Classification (MUSIC) often rely heavily on accurate prior information. In this paper, we propose a novel underwater electric field location algorithm to accurately locate an unknown number of targets. This paper constructs a complete output model of electric field detection array in the spatial domain based on Sparse Bayesian Learning (SBL), and transforms the target location problem into sparse signal reconstruction problem. The experimental results demonstrate the effectiveness of the proposed method and its advantages over the MUSIC algorithm. The proposed location algorithm is capable of accurately locating an unknown number of ships and other targets.

Keywords: Extremely low frequency electric field, Sparse signal, Target location, Sparse Bayesian learning, Multiple signal classification.

1. INTRODUCTION

On ships and underwater vehicles, ELF electric field is generated under the modulated influence of the propeller due to the current induced by seawater corrosion and anodic protection system. The ELF electric field signal contains rich target information such as propeller speed, heading, and position, and is a key exposed signal for ships and other targets, which can be used for underwater target detection, location and identification [1]-[4]. Compared to acoustic and other non-acoustic methods, the underwater ELF electric field signal offers stronger resistance to noise, longer propagation distance, simpler detection equipment, and better concealment [5]-[7].

Currently, passive electric field location methods for stationary targets on underwater vehicles primarily rely on array processing algorithms [8]-11]. These algorithms estimates the target's position by leveraging the amplitude differences of the target's electric field across the detection array, combined with conventional radar array signal processing techniques. Xue *et al*. applied the MUSIC algorithm to near-field underwater location, but this method has certain limitations in practical implementation [12]. Subsequently, Xu *et al*. proposed a new method for electric dipole source location based on boundary element method theory and multi-signal classification, which enables fast target location through a global multi-region conjugate gradient hybrid search [13]. The following year, Xu *et al*. introduced the mirror principle into the array manifold and employed a fast optimization method based on an improved matrix adaptive evolutionary strategy to locate the target [14]. Further, Ci *et al*. analyzed the horizontal and non-horizontal states. For dipoles in the horizontal state, position estimation is performed using binary image boundary extraction, least-squares linear fitting, and the Gauss-Newton iterative method. For dipoles in the non-horizontal state, position estimation is performed using the multi-polarized MUSIC algorithm combined with the particle swarm optimization algorithm [15].

Array processing methods offer high location accuracy, but they rely on prior information about the number of targets. Inaccurate estimation of the target count can significantly affect the accuracy of target estimation [16], [17]. SBL, which has emerged in recent years, offers a solution to this problem, as shown in Figure **1**. The main contributions of this paper are as follows:

1) This paper develops a complete output model for the electric field detection array based on sparse reconstruction theory.

2) This paper transforms the target location problem into a sparse signal reconstruction problem, and proposes a multi-target electric field location method based on SBL.

3) Experimental results validate the effectiveness of the proposed algorithm and demonstrate its superiority over the MUSIC algorithm.

2. PROPOSED ELECTRIC FIELD LOCATION METHOD

2.1. Spatial Complete Representation of Array Output

Suppose that there are K electric dipole targets at different positions $\boldsymbol{R}=\left(\boldsymbol{r}_1,\boldsymbol{r}_2,\boldsymbol{r}_3,\cdots,\boldsymbol{r}_K\right)$, incident on an electrode array composed of M sensors at time

*Address correspondence to this author at the Xi'an Jiaotong University, 28 Xianning West Road, Xi'an 710049, China;
E-mail: hqxjtu@xjtu.edu.cn

E-ISSN: 2409-9694/24

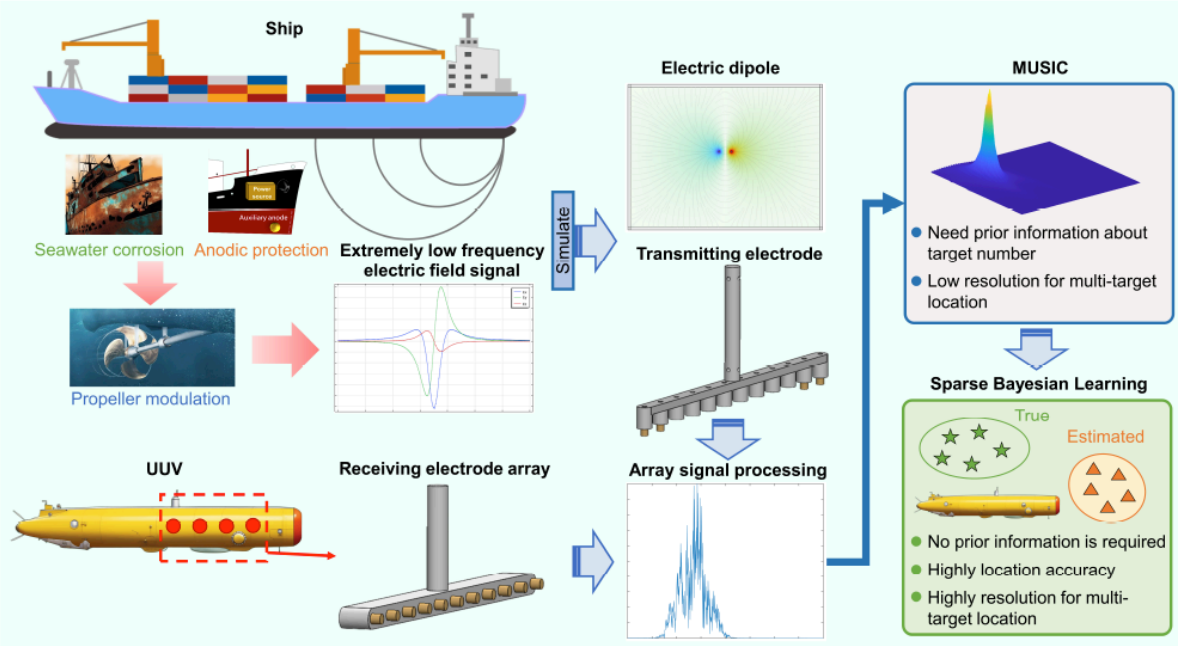

Figure 1: The proposed multi-target location solution for underwater electrosense robots.

$\boldsymbol{r}_k=\left(x_k,y_k\right)^T$, where $M<K$. The output on the array at time t is:

$$\boldsymbol{x}(t)=\sum_{k=1}^{K}\boldsymbol{\varphi}\left(\boldsymbol{r}_k\right)s_k(t)+\boldsymbol{v}(t) \tag{1}$$

where $\boldsymbol{x}(t)=\left[x_1(t),\cdots,x_M(t)\right]^T$. $\boldsymbol{\varphi}\left(\boldsymbol{r}_k\right)$ is the array response vector of the $k\text{-}th$ signal. $s_k(t)$ is the waveform of the $k\text{-}th$ signal at time t. $\boldsymbol{v}(t)$ is Gaussian white noise with zero mean and σ_n power received at time t.

For the convenience of subsequent analysis, the observed noise at different times and on different sensors is assumed to be independent. When the L group of time $t=t_1,t_2,\cdots t_L$ is taken rapidly, (1) can be written in vector form:

$$\boldsymbol{X}=\boldsymbol{\Psi}(\boldsymbol{R})\boldsymbol{S}+\boldsymbol{V} \tag{2}$$

where $\boldsymbol{X}=\left[\boldsymbol{x}(t_1),\cdots,\boldsymbol{x}(t_L)\right]$ is the output matrix of $M\times L$ dimension electrode array. $\boldsymbol{\Psi}(\boldsymbol{R})=\left[\boldsymbol{\varphi}(r_1),\mathrm{L}\ ,\boldsymbol{\varphi}(\boldsymbol{r}_K)\right]$ is the $M\times K$ dimension electrode array response matrix. $\boldsymbol{S}=\left[\boldsymbol{s}(t_1),\cdots,\boldsymbol{s}(t_L)\right]$ is the signal waveform matrix of $K\times L$ dimension. $\boldsymbol{V}=\left[\boldsymbol{v}(t_1),\cdots,\boldsymbol{v}(t_L)\right]$ is the Gaussian white noise of $M\times L$ dimension.

The reason sparse reconstruction theory can be applied to the passive location of underwater electric field using an electrode array is that the incident signal from the target exhibits spatial sparsity, as shown in Figure **2**. By dividing the detection region into $\left\{\tilde{\boldsymbol{r}}_1,\tilde{\boldsymbol{r}}_2,\cdots\tilde{\boldsymbol{r}}_N\right\}$ equal intervals across the entire space, a complete position set $\tilde{\boldsymbol{R}}=\left[\tilde{\boldsymbol{r}}_1,\tilde{\boldsymbol{r}}_2,\cdots\tilde{\boldsymbol{r}}_N\right]1$ is obtained, where $K<M\ll N$ makes the target location $\boldsymbol{R}=\left(\boldsymbol{r}_1,\boldsymbol{r}_2,\boldsymbol{r}_3,\cdots\boldsymbol{r}_K\right)$ a subset of the set. Compared to the spatially complete location set, the number of target position is small and limited. If the signal energy corresponding to the non-existent target positions is treated as zero, the signal energy corresponding to the spatially complete position set forms a sparse vector. The target signal can be recovered using sparse reconstruction methods, allowing for target location estimation.

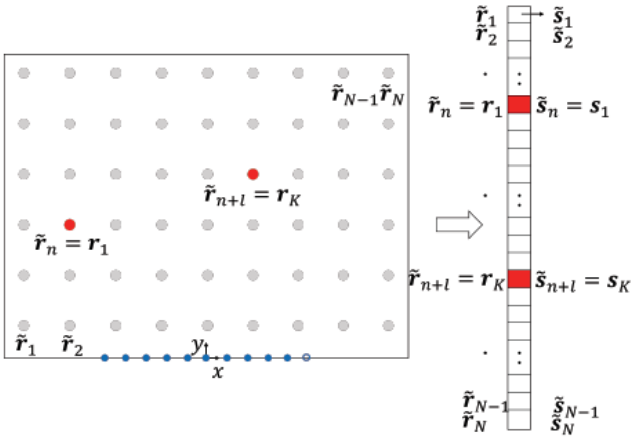

Figure 2: Spatial sparse representation of array signal.

Equation (1) can be extended to obtain a complete array output model:

$$\boldsymbol{x}(t)=\sum_{i=1}^{N}\varphi(\tilde{\boldsymbol{r}}_i)\tilde{s}_k(t)+\boldsymbol{\nu}(t) \tag{3}$$

The non-zero value $\tilde{s}_n(t)=s_k(t)$ is taken if and only if $\tilde{\boldsymbol{r}}_n=\boldsymbol{r}_k$, and the corresponding output form of the complete array under the multi-beat condition is as follows:

$$\boldsymbol{X}=\bar{\boldsymbol{\Psi}}(\tilde{\boldsymbol{r}}_s)\bar{\boldsymbol{S}}+\boldsymbol{V} \tag{4}$$

where $\bar{\boldsymbol{\Psi}}(\tilde{\boldsymbol{R}})=\left[\varphi(\tilde{\boldsymbol{r}}_1),\cdots,\varphi(\tilde{\boldsymbol{r}}_N)\right]$ is referred to as a spatially complete dictionary set, abbreviated as $\bar{\boldsymbol{\Psi}}$, and its columns are referred to as basis functions. The term "complete" means that the number of columns is typically greater than the number of rows. $\bar{\boldsymbol{S}}=\left[\bar{\boldsymbol{s}}(t_1),\bar{\boldsymbol{s}}(t_2),\cdots,\bar{\boldsymbol{s}}(t_L)\right]$ is a zero-complement extension of the signal vector $\bar{\boldsymbol{S}}$, extending from $\boldsymbol{R}$ to $\tilde{\boldsymbol{R}}$, and is referred to as a spatially complete signal set. The positions of non-zero values in $\bar{\boldsymbol{s}}(t_l)$ at different times correspond to the positions $\boldsymbol{r}_k$ of each signal. Therefore, if the target position remains unchanged during the positioning process, the number of non-zero elements in $\bar{\boldsymbol{S}}=\left[\bar{\boldsymbol{s}}(t_1),\bar{\boldsymbol{s}}(t_2),\cdots,\bar{\boldsymbol{s}}(t_L)\right]$ also remains constant. Only the element values at K positions where the target actually exists are non-zero, while the element values at the other $N-K$ positions are zero.

By converting the output model on the array in (1) into the spatially complete output model in (4), the target position estimation problem is transformed into the optimal fitting problem of $\bar{\boldsymbol{\Psi}}\bar{\boldsymbol{S}}$ and $\boldsymbol{X}$ by selecting K basis functions from the spatially complete dictionary set $\bar{\boldsymbol{\Psi}}$, where the K basis functions correspond to K target positions one by one. To ensure the universality of the model, no prior information regarding the target position or number is provided, and the complete location set $\tilde{\boldsymbol{R}}=\left[\tilde{\boldsymbol{r}}_1,\tilde{\boldsymbol{r}}_2,\cdots\tilde{\boldsymbol{r}}_N\right]$ is obtained by uniformly sampling the target detection region.

2.2. Location Methods Based on SBL

In the matrix output spatially complete model (4), since $K<M\ll N$, that is, the dimension of $\bar{\boldsymbol{S}}$ is much greater than the number of non-zero rows, resulting in strong sparsity in the spatially complete model. The problem of recoverinμg the target signal and estimating the target position from it is known as the sparse reconstruction problem, which can be expressed as:

$$\begin{aligned}&\min_{\bar{\boldsymbol{S}}}\left\|\bar{\boldsymbol{S}}\right\|_{0,2}\\&s.t.\left\|\boldsymbol{X}-\bar{\boldsymbol{\Psi}}\bar{\boldsymbol{S}}\right\|_F^2\le\varepsilon\end{aligned} \tag{5}$$

where $\left\|\boldsymbol{X}-\bar{\boldsymbol{\Psi}}\bar{\boldsymbol{S}}\right\|_F$ is the Frobenius norm of $\boldsymbol{X}-\bar{\boldsymbol{\Psi}}\bar{\boldsymbol{S}}$, representing the fitting error between the spatial complete model and the observed data from the electrode array, essentially acting as a constraint on the noise. ε is the energy upper bound of noise. $\left\|\bar{\boldsymbol{S}}\right\|_{0,2}$ is the $l_{0,2}$ norm of the matrix $\bar{\boldsymbol{S}}$, which corresponds to the number of non-zero rows, and can be expressed as:

$$\left\|\bar{\boldsymbol{S}}\right\|_{0,2}@\left\|\left[\left\|\left[\bar{\boldsymbol{S}}\right]_{1,:}\right\|_2,\cdots,\left\|\left[\bar{\boldsymbol{S}}\right]_{N,:}\right\|_2\right]^T\right\|_0 \tag{6}$$

where $\left\|\left[\bar{\boldsymbol{S}}\right]_{n,:}\right\|_2$ is the l_2 norm of the n row vector in the matrix $\bar{\boldsymbol{S}}$.

A sparse solution that reflects the actual number and positions of the objects can be obtained by solving (5). However, because the l_0 norm is a non-convex function, its solution is a NP-Hard problem, and there is no efficient and simple solution method [18]-21]. SBL is the only sparse reconstruction method that exhibits global convergence similar to the l_0 norm by exploiting the sparse characteristics of the target space and combining prior information with posterior probabilities to reconstruct each signal component [22]. Therefore, this paper adopts the SBL method to estimate the target position. Specifically, an intermediate parameter $\gamma=\left[\gamma_1,\gamma_2,\cdots,\gamma_N\right]$ is introduced into the array's complete output model (4), with the assumption that:

$$\bar{\boldsymbol{s}}(t_l)\sim N(0,\Gamma),l=1,2,3,\cdots,L \tag{7}$$

where $N(0,\Gamma)$ follows a Gaussian distribution with zero mean and Γ variance, and $\Gamma=\mathrm{diag}(\gamma)$. The row sparsity of $\bar{\boldsymbol{S}}$ is controlled by the parameter γ. When $\gamma_n=0$, the $n\text{-}th$ row elements in matrix $\bar{\boldsymbol{S}}$ are all zero, meaning that $\bar{\boldsymbol{S}}$ and γ share the same target spatial distribution information. To ensure the accurate reconstruction of the spatial characteristics of each target signal, it is assumed that the variables $\bar{\boldsymbol{s}}(t_l)$ at different time instances in Equation (7) are mutually independent. In addition, since the observed noise $\boldsymbol{\nu}$ also follows a Gaussian distribution with zero mean and power σ_n, $\bar{\boldsymbol{s}}(t_l)$ and $\boldsymbol{\nu}$ form a conjugate distribution pair, which helps simplify the subsequent calculation.

Based on the above analysis, it can be seen that both the probability density $p\left(\bar{\boldsymbol{S}}\right)$ of $\bar{\boldsymbol{S}}$ and the likelihood function $p(\boldsymbol{X}\mid\bar{\boldsymbol{S}};\sigma_n^2)$ of the observed data follow a Gaussian distribution:

$$p\left(\bar{\boldsymbol{S}}|\boldsymbol{\gamma}\right)=\left|\pi\boldsymbol{\Gamma}\right|^{-L}e^{\left[-tr\left(\bar{\boldsymbol{S}}^H\boldsymbol{\Gamma}^{-1}\bar{\boldsymbol{S}}\right)\right]} \tag{8}$$

$$p\left(\boldsymbol{X}|\bar{\boldsymbol{S}};\sigma_n^2\right)=\left|\pi\sigma_n^2\boldsymbol{I}_M\right|^{-L}e^{\left[-\sigma_n^2\left\|X-\bar{\boldsymbol{A}}\bar{\boldsymbol{S}}\right\|_F^2\right]} \tag{9}$$

According to Bayes' theorem, the posterior probability $p(\bar{\boldsymbol{S}}\mid\boldsymbol{X};\gamma,\sigma_n^2)$ of $\bar{\boldsymbol{S}}$ with respect to $\boldsymbol{X}$ is:

$$p\left(\bar{\boldsymbol{S}}|\boldsymbol{X};\boldsymbol{\gamma},\sigma_n^2\right)=\frac{p\left(\boldsymbol{X}|\bar{\boldsymbol{S}};\sigma_n^2\right)p\left(\bar{\boldsymbol{S}}|\boldsymbol{\gamma}\right)}{\int p\left(\boldsymbol{X}|\bar{\boldsymbol{S}};\sigma_n^2\right)p\left(\bar{\boldsymbol{S}}|\boldsymbol{\gamma}\right)d\bar{\boldsymbol{S}}}=\left|\pi\boldsymbol{\Sigma}_{\bar{\boldsymbol{S}}}\right|^{-L}e^{\left\{-tr\left[\left(\bar{\boldsymbol{S}}-\boldsymbol{\mu}_{\bar{\boldsymbol{S}}}\right)^H\boldsymbol{\Sigma}_{\bar{\boldsymbol{S}}}^{-1}\left(\bar{\boldsymbol{S}}-\boldsymbol{\mu}_{\bar{\boldsymbol{S}}}\right)\right]\right\}} \tag{10}$$

$$\boldsymbol{\mu}_{\bar{\boldsymbol{S}}}=\boldsymbol{\Gamma}\bar{\boldsymbol{A}}^H\left(\sigma_n^2\boldsymbol{I}+\bar{\boldsymbol{A}}\boldsymbol{\Gamma}\bar{\boldsymbol{A}}^H\right)^{-1}\boldsymbol{X} \tag{11}$$

$$\boldsymbol{\Sigma}_{\bar{\boldsymbol{S}}}=\boldsymbol{\Gamma}-\boldsymbol{\Gamma}\bar{\boldsymbol{A}}^H\left(\sigma_n^2\boldsymbol{I}+\bar{\boldsymbol{A}}\boldsymbol{\Gamma}\bar{\boldsymbol{A}}^H\right)^{-1}\bar{\boldsymbol{A}}\boldsymbol{\Gamma} \tag{12}$$

Under the given medium parameters γ and σ_n^2, by maximizing (10), the maximum posterior estimate $\mu_{\bar{\boldsymbol{S}}}$ of the signal can be obtained according to (11). However, the accuracy of the reconstruction results depends on the appropriateness of the prior distribution in (8). Only when γ accurately reflects the target position distribution can the signal be correctly reconstructed through (9). Therefore, the value of γ is optimized using the array observation data to enhance its appropriateness. Specifically, the known likelihood function of $\boldsymbol{X}$ with respect to γ is:

$$p\left(\boldsymbol{X}|\boldsymbol{\gamma};\sigma_n^2\right)=\int p\left(\boldsymbol{X}|\bar{\boldsymbol{S}};\sigma_n^2\right)p\left(\bar{\boldsymbol{S}}|\boldsymbol{\gamma}\right)d\bar{\boldsymbol{S}}=\left|\pi\boldsymbol{\Sigma}_{\boldsymbol{X}}\right|^{-N}e^{\left[-tr\left(\boldsymbol{X}^H\boldsymbol{\Sigma}_{\boldsymbol{X}}^{-1}\boldsymbol{X}\right)\right]} \tag{13}$$

$$\sum_{\boldsymbol{X}}=\sigma_n^2\boldsymbol{I}+\bar{\boldsymbol{A}}\boldsymbol{\Gamma}\bar{\boldsymbol{A}}^H \tag{14}$$

Taking the logarithm of (13) and ignoring the constant term, we obtain the objective function for optimizing γ:

$$L\left(\boldsymbol{\gamma},\sigma_n^2\right)=\ln\left|\boldsymbol{\Sigma}_{\boldsymbol{X}}\right|+tr\left(\boldsymbol{\Sigma}_{\boldsymbol{X}}{}^{-1}\hat{\boldsymbol{R}}\right) \tag{15}$$

where $\hat{\boldsymbol{R}}=\boldsymbol{X}\boldsymbol{X}^H/L$ is the covariance matrix estimate of the array observation data. The estimated value $\hat{\boldsymbol{\gamma}}$ of γ can be obtained by minimizing Equation (15), which provides reasonable prior distribution information for accurate reconstruction of the target signal.

The premise of the above optimization process is that the noise power is known. Since the estimated noise power significantly affects the signal reconstruction accuracy, it is necessary to jointly estimate the noise power during the solution process. Therefore, an Expectation Maximization (EM) algorithm with guaranteed convergence is used to solve the problem.

In EM algorithm, parameters $\gamma^{(0)}$ and $\left(\sigma_n^2\right)^{(0)}$ are first initialized. In $E\text{-}step$, the first and second moments of $\bar{\boldsymbol{S}}$ are obtained by maximizing (10), which corresponds to (11) and (12). Then in $E\text{-}step$, through $\frac{\partial L\left(\gamma,\sigma_n^2\right)}{\partial\gamma}=0$ and $\frac{\partial L\left(\gamma,\sigma_n^2\right)}{\partial\sigma_n^2}=0$, parameters $\gamma^{(i)}$ and $\left(\sigma_n^2\right)^{(i)}$ of the $i\text{-}th$ iteration are obtained:

$$\gamma_n^{(i)}=\frac{\left\|\left(\boldsymbol{\mu}_{\bar{\boldsymbol{S}}}^{(i)}\right)_{n,:}\right\|_2^2}{N}+\left(\boldsymbol{\Sigma}_{\bar{\boldsymbol{S}}}^{(i)}\right)_{n,n}\quad s,n=1,2,\mathrm{L}\ ,N \tag{16}$$

$$\left(\sigma_n^2\right)^{(i)}=\frac{\left\|\boldsymbol{X}-\bar{\boldsymbol{A}}\boldsymbol{\mu}_{\bar{\boldsymbol{S}}}^{(i)}\right\|_F^2/L}{M-N+\sum_{n=1}^{N}\left(\boldsymbol{\Sigma}_{\bar{\boldsymbol{S}}}^{(i)}\right)_{n,n}/\gamma_n} \tag{17}$$

where $\boldsymbol{\mu}_{\bar{\boldsymbol{S}}}^{(i)}$ and $\boldsymbol{\Sigma}_{\bar{\boldsymbol{S}}}^{(i)}$ are given by (11) and (12). $\left(\boldsymbol{\mu}_{\bar{\boldsymbol{S}}}^{(i)}\right)_{n,:}$ is the $n\text{-}th$ row of $\boldsymbol{\mu}_{\bar{\boldsymbol{S}}}^{(i)}$. $\left(\boldsymbol{\Sigma}_{\bar{\boldsymbol{S}}}^{(i)}\right)_{n,n}$ is the $n\text{-}th$ row and $n\text{-}th$ column element of $\boldsymbol{\Sigma}_{\bar{\boldsymbol{S}}}^{(i)}$. When the results of the alternating iterations of γ and σ_n^2 satisfy the convergence condition, the estimated value $\hat{\boldsymbol{\gamma}}$ for the intermediate parameter γ, which contains the target position and the estimated noise power $\hat{\sigma}_n^2$, is obtained. The maximum posterior estimate of $\hat{\boldsymbol{\mu}}_{\bar{\boldsymbol{S}}}$ for the target signal can be obtained by substituting the Equation (11). The target position estimation can be achieved by performing a maximum (spectral peak) search for $\hat{\boldsymbol{\gamma}}$ or $\hat{\boldsymbol{\mu}}_{\bar{\boldsymbol{S}}}$.

The initialization method for the initial values of parameters γ and σ_n^2, is as follows:

$$\boldsymbol{\mu}_{\bar{\boldsymbol{S}}}{}^{(0)}=\bar{\boldsymbol{A}}^H\left(\bar{\boldsymbol{A}}\bar{\boldsymbol{A}}^H\right)^{-1}\boldsymbol{X} \tag{18}$$

$$\gamma_n^{(0)}=\frac{\left\|\left(\boldsymbol{\mu}_{\bar{\boldsymbol{S}}}{}^{(0)}\right)_{n\cdot}\right\|_2^2}{L} \tag{19}$$

$$\left(\sigma_n^2\right)^{(0)}=\frac{\left\|\boldsymbol{X}\right\|_F^2}{ML} \tag{20}$$

In summary, the specific process of the underwater multi-target electric field location algorithm based on SBL is outlined as follows:

Step1. Specify the detection area and uniformly sample it to obtain a complete position set $\tilde{\boldsymbol{R}}$;

Step2. Based on the underwater electric field distribution model of electric dipoles and the position of the electrode array, we obtain a spatially complete dictionary set $\bar{\boldsymbol{\Psi}}$.

Step3. Initialize the parameters $\boldsymbol{\gamma}^{(0)}$ and $\left(\sigma_n^2\right)^{(0)}$ according to (19) and (20), and determine the maximum number of iterations $i_{\max}$ and the convergence threshold $\xi_{\min}$.

Step4. Update $\boldsymbol{\gamma}^{(i)}$ and $\left(\sigma_n^2\right)^{(i)}$ according to (17) and (18).

Step5. Stop the iteration when $i \geq i_{\max}$ or $\xi = \left\|\boldsymbol{\gamma}^{(i)} - \boldsymbol{\gamma}^{(i-1)}\right\|_2 / \left\|\boldsymbol{\gamma}^{(i-1)}\right\|_2 \leq \xi_{\min}$ is satisfied and obtain the dipole source position by searching for the spectral peak of $\hat{\boldsymbol{\gamma}}$.

3. EXPERIMENT AND RESULTS

3.1. Electrode System

The electrode system consists of two parts: the transmitting electrode and the receiving electrode array. The transmitting electrode simulates the target to generate the ELF electric field and consists of 2 pairs of electrodes with a spacing of 40 mm. The spacing between the two pairs of electrodes is adjustable. The receiving electrode array receives the electric field signal generated by the target. It consists of 11 electrodes, including 1 reference electrode (the blue hollow circle in Figure **2**.) and 10 effective electrodes, with an electrode spacing of 40 mm. The properties of electrode materials have a significant impact on the overall detection performance. Considering the material's requirements of self-noise, stability, oxidation resistance, corrosion resistance, and range drift, the titanium electrode was selected as the sensing unit in this paper. The titanium electrode was installed on the 3D printed stand to complete the construction of the transmitting electrode and the receiving electrode array, as shown in Figure **3**.

3.2. Experiment Platform

The experimental platform for the electric dipole source location experiment is shown in Figure **4**. It consists of a receiving electrode array, transmitting electrode, signal generator, 3D slide table, National Instruments (NI) data acquisition device, power amplifier, motion controller, and other components.

The experimental platform has dimensions of (2.4×1.2×1) m^3, with the transmitting electrode fixed on the three-dimensional sliding platform via an acrylic tube. The sinusoidal signal generated by the signal generator is amplified by the power amplifier to produce a pair of differential signals, which are applied to the two electrodes of the transmitting electrode. The

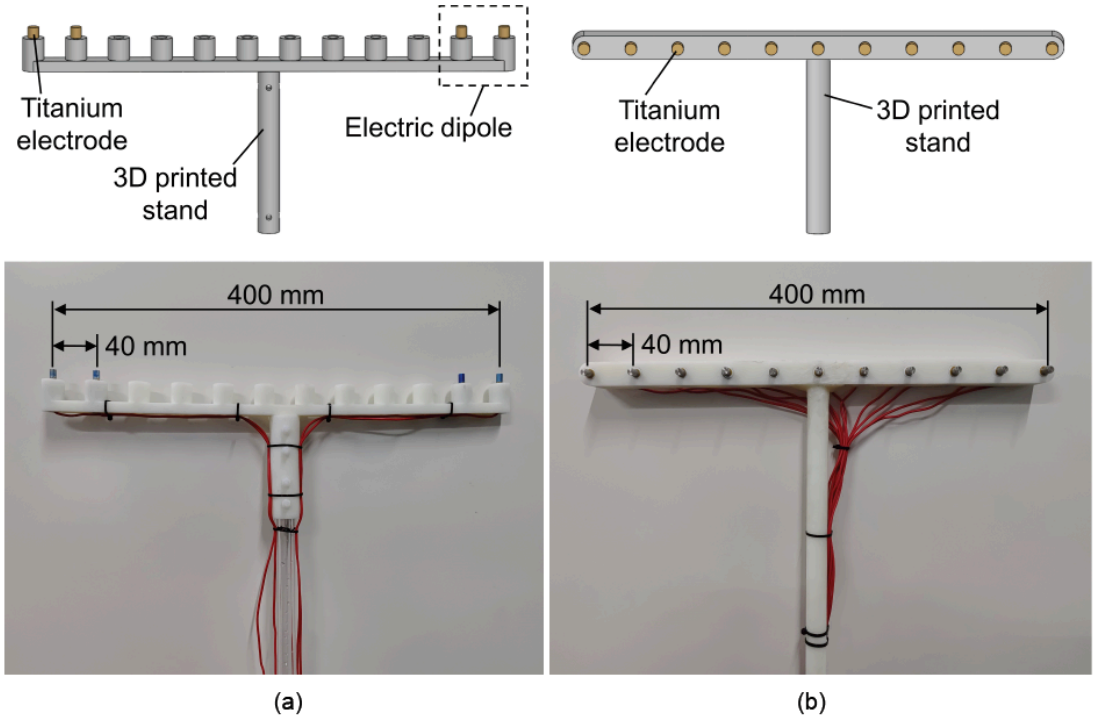

Figure 3: Electrode system. (**a**) Transmitting electrode. (**b**) Receiving electrode array.

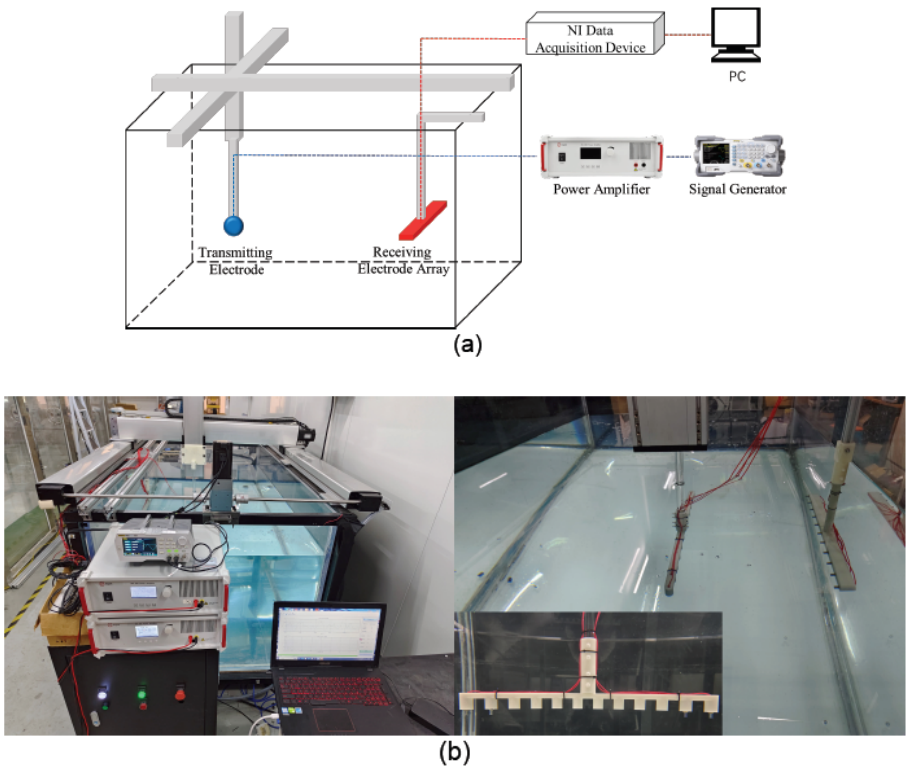

Figure 4: Experimental setup. (**a**) Equipment composition. (**b**) Experimental facilities

detection array is fixed along the long side of the pool using an aluminum profile, and the electric field signals it receives are collected and stored by the data acquisition card.

Figure **2(a)** shows the experimental setup for the double electric dipole target. The frequencies of the electric dipole targets are 14 Hz and 20 Hz, and their electric dipole moment is 0.0042 A·m. The sampling rate of the NI data acquisition system is 2000 Hz, with a sampling duration of 150 seconds. The water conductivity is 0.08 S/m.

3.3. Multi-Target Location Results

The MUSIC and SBL algorithms are used to locate the double electric dipole targets at six different positions.

The location results are shown in Figure **5** and Figure **6**. The SBL algorithm successfully locates all six

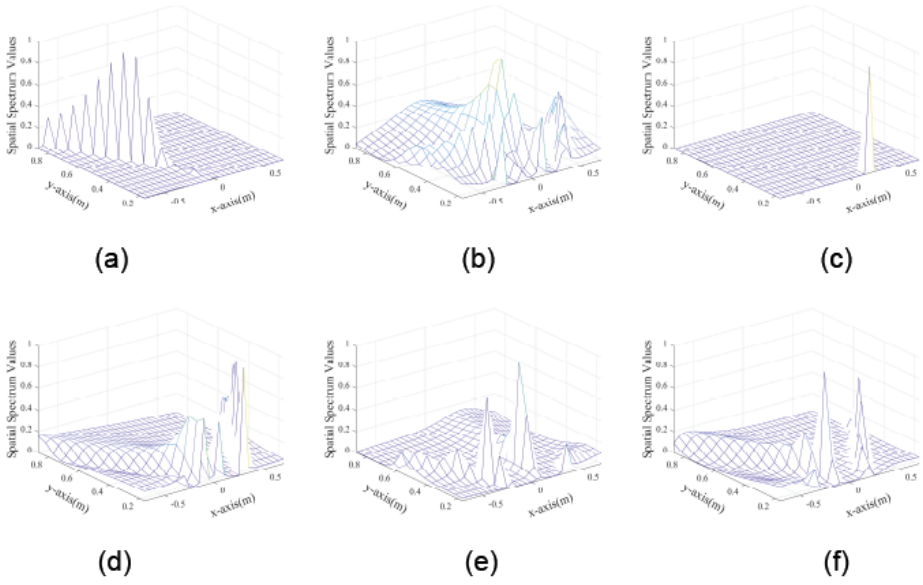

Figure 5: Location results of the MUSIC algorithm. (**a**) Position 1. (**b**) Position 2. (**c**) Position 3. (**d**) Position 4. (**e**) Position 5. (**f**) Position 6.

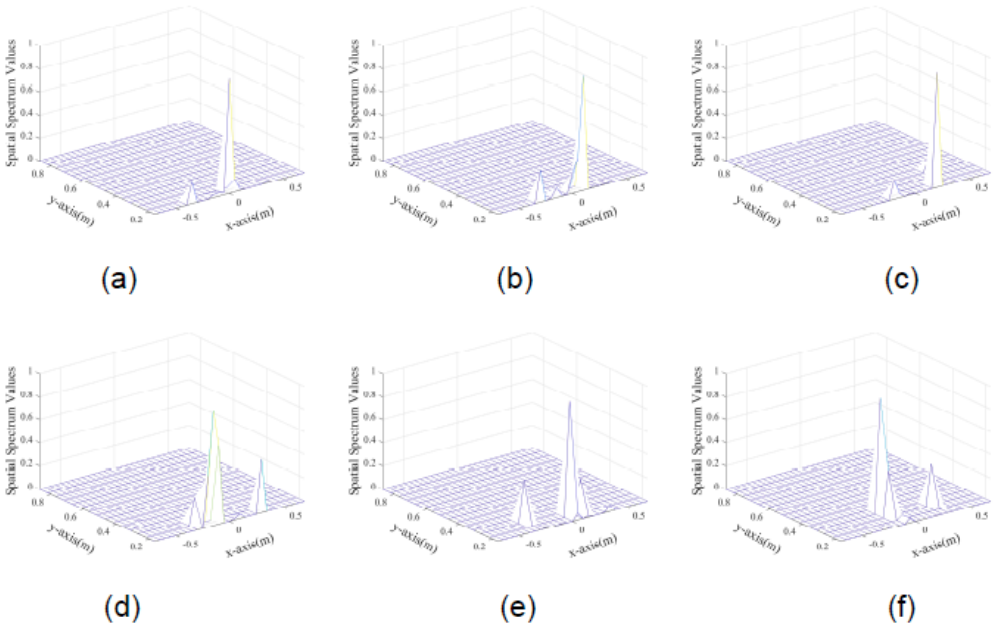

Figure 6: Location results of the SBL algorithm. (**a**) Position 1. (**b**) Position 2. (**c**) Position 3. (**d**) Position 4. (**e**) Position 5. (**f**) Position 6.

targets, while the MUSIC algorithm locates only four, with a failure at position 1 and position 3. In terms of target resolution, the SBL algorithm offers higher resolution and can effectively distinguish between two different targets, while the MUSIC algorithm struggles to differentiate them.

The specific location results are shown in Table **1**. In terms of effective location error, the maximum estimated error for the MUSIC algorithm is 0.4272 m, while the maximum estimated error for the SBL algorithm is 0.1118 m. For the five positions where both the MUSIC and SBL algorithms successfully locate the targets, the average error for MUSIC is 0.1088 m, whereas for SBL, it is 0.0312 m. Clearly, the SBL algorithm outperforms the MUSIC algorithm.

Based on the above location experiment results, the SBL algorithm clearly outperforms the MUSIC algorithm and can achieve accurate target location even when the number of targets is unknown, making it more practical. The proposed method exhibits superior performance in multi-target estimation. This occurs because when the targets are located in close proximity, the correlation between their signals increases, which reduces the accuracy of the array signal covariance matrix and subspace estimation. This, in turn, leads to degraded performance or even failure

Table 1: Comparison of Experimental Results of Dual Target Location

Target Position	MUSIC	Error	SBL	Error
(-0.4m,0.17m), (0m,0.17m)	—	—	(-0.35m,0.17m), (0m,0.17m)	0.0508m, 0m
(-0.3m,0.17m), (0.1m,0.17m)	(0m,0.37m), (0.5m,0.32m)	0.3606m, 0.4272m	(-0.3m,0.17m), (0.1m,0.17m)	0m, 0m
(-0.2m,0.17m), (0.2m,0.17m)	— (0.2m,0.17m)	— 0m	(-0.2m,0.17m), (0.2m,0.17m)	0m, 0m
(-0.1m,0.17m), (0.3m,0.17m)	(-0.1m,0.17m), (0.3m,0.17m)	0m, 0m	(-0.15m,0.27m), (0.3m,0.27m)	0.1118m, 0.1m
(-0.3m,0.27m), (0.1m,0.27m)	(-0.3m,0.27m), (0.1m,0.32m)	0m, 0.05m	(-0.3m,0.27m), (0.05m,0.27m)	0m, 0.05m
(-0.1m,0.27m), (0.3m,0.27m)	(-0.1m,0.27m), (0.4m,0.37m)	0m, 0.1414m	(-0.1m,0.32m), (0.3m,0.27m)	0.05m, 0m

of the MUSIC algorithm. In contrast, the SBL algorithm estimates target locations by fitting the observed data to a set of basis functions, eliminating the need for eigenvalue decomposition.

5. CONCLUSION

In this paper, an electric dipole source location method based on SBL is proposed to address the limitations of current underwater multi-target passive electric field location methods. The experimental results demonstrate that the SBL algorithm can accurately estimate both the number and positions of targets, even when the number of targets and the intensity of the signal source are unknown. In the location experiment of the double dipole target at different positions, the MUSIC algorithm can achieve effective location for only five positions, while the SBL algorithm successfully locates all six positions. For the five positions where both the MUSIC and SBL algorithms successfully locate the targets, the average error for MUSIC is 0.1088 m, while for SBL it is 0.0312 m, which is 71.32% lower than that of MUSIC. In the future, we aim to mount electrode arrays on underwater motion platforms to investigate the effects of platform motion and seawater flow. The proposed method holds significant potential for application in Underwater Unmanned Vehicles (UUVs) and Remotely Operated Vehicles (ROVs).

ACKNOWLEDGMENTS

This work was supported by Ye Qisun Science Foundation of National Natural Science Foundation of China (Grant No. U2441288) and the National Natural Science Foundation of China (Grant No. 52371337).

CONFLICTS OF INTEREST

All authors disclosed no relevant relationships.

REFERENCES

[1] Cheng JF, Yu P, Zhang JW, *et al*. Application and development of underwater electric field detection and location technology. Journal of Naval University of Engineering 34(04), 68-69 (2022).

[2] Zhao WC, Jiang RX, Yu P, *et al*. Detection and identification of ship shaft-rate electric field based on line-spectrum characteristics. Acta Armamentarii 41(6), 1165-1171 (2020).

[3] Yaakobi O, Zilman G, Miloh T. Detection of the electromagnetic field induced by the wake of a ship moving in a moderate sea state of finite depth. Journal of Engineering Mathematics 70, 17-27 (2011). https://doi.org/10.1007/s10665-010-9410-z

[4] Zhang JW, Jiang RX, Gong SG. Study of the electric field induced by the wake of a moving ship. Journal of Harbin Engineering University 35(8), 931-935 (2014).

[5] Bai JX, Gong SG. Physical field of ship. The Publishing House of Ordnance Industry, Beijing (2007).

[6] Wang KS, Zhou GH, Zeng WS, *et al*. Detection of ship shaft-rate electromagnetic field signal based on NLMS algorithm. In: 2021 7th International Symposium on Sensors, Mechatronics and Automation System (ISSMAS). 1846 012097. J. Phys (2021). https://doi.org/10.1088/1742-6596/1846/1/012097

[7] Cheng JF, Zhang JW, Jiang RX, *et al*. Development status of underwater electromagnetic detection technology. Digital Ocean & Underwater Warfare 2(04), 45-49 (2022).

[8] Liu Q, Sun Z, Jiang R, *et al*. Electric field detection system based on denoising algorithm and high-speed motion platform. Sensors 22(14), 5118 (2022). https://doi.org/10.3390/s22145118

[9] Shang W, Xue W, Li Y, *et al*. An improved underwater electric field-based target localization combining subspace scanning algorithm and Meta-EP PSO algorithm. Journal of Marine Science and Engineering 8(4), 232 (2020). https://doi.org/10.3390/jmse8040232

[10] Liu Q, Sun ZL, Jiang RX, *et al*. Tracking model of joint electromagnetic signals of naval targets based on small-scale platform. Progress In Electromagnetics Research C 122, 199-213 (2022). https://doi.org/10.2528/PIERC22060201

[11] Wang H, Wang X, Zhang J. Research on positioning of surface warships in shallow water based on circular array. In: 2019 IEEE 8th Joint International Information Technology and Artificial Intelligence Conference (ITAIC). pp. 450-453. IEEE (2019). https://doi.org/10.1109/ITAIC.2019.8785581

[12] Xue B, Qu XD, Fang GY, *et al*. Research and analysis on the localization of a 3-D single source in lossy medium using uniform circular array. Sensors 17(6), 1274 (2017). https://doi.org/10.3390/s17061274

[13] Xu YD, Xue W, Li YS, *et al*. Shang. Multiple signal classification algorithm based electric dipole source localization method in an underwater environment. Symmetry 9(10), 231 (2017). https://doi.org/10.3390/sym9100231

[14] Xu YD, Guo LL, Shang WJ, *et al*. Li. Underwater electro-location method based on improved matrix adaptation evolution strategy. IEEE Access 6, 39220-39232 (2018). https://doi.org/10.1109/ACCESS.2018.2855965

[15] Ci LF, Xue W, Dang JH, *et al*. Underwater target electric field location algorithm based on electric dipole. In: 2022 IEEE Asia-Pacific Conference on Image Processing, Electronics and Computers (IPEC). pp. 222-227. IEEE (2022). https://doi.org/10.1109/IPEC54454.2022.9777456

[16] Wipf DP, Rao BD. Sparse Bayesian learning for basis selection. IEEE Transactions on Signal Processing 52(8), 2153-2164 (2004). https://doi.org/10.1109/TSP.2004.831016

[17] Gerstoft P, Mecklenbräuker CF, Xenaki A, *et al*. Multisnapshot Sparse Bayesian Learning for DOA. IEEE Signal Processing Letters 23(10), 1469-1473 (2016). https://doi.org/10.1109/LSP.2016.2598550

[18] Portilla J, Mancera L. L0-based sparse approximation: two alternative methods and some applications. In: Optical Engineering and Applications. pp. 1-15. Proc. SPIE 6701 (2007). https://doi.org/10.1117/12.736231

[19] Mohimani H, Zadeh MB, Jutten C. A fast approach for overcomplete sparse decomposition based on smoothed l_0 norm. IEEE Trans. Signal Processing 57(1), 289-301 (2009). https://doi.org/10.1109/TSP.2008.2007606

[20] Hyder MM, Mahata K. An improved smoothed l_0 approximation algorithm for sparse representation. IEEE Trans. Signal Processing, 58(4), 2194-2205 (2010). https://doi.org/10.1109/TSP.2009.2040018

[21] Mourad N, Reilly JP. Minimizing nonconvex functions for sparse vector reconstruction. IEEE Trans. Signal Processing 58(7), 3485-3496 (2010). https://doi.org/10.1109/TSP.2010.2046900

[22] Kim JM, Lee OK, Ye JC. Compressive MUSIC: Revisiting the link between compressive sensing and array signals processing. IEEE Transactions Information Theory 58(1), 278-300 (2012). https://doi.org/10.1109/TIT.2011.2171529

Received on 17-11-2024 Accepted on 20-12-2024 Published on 29-12-2024

https://doi.org/10.31875/2409-9694.2024.11.11